IEEE Access
Multidisciplinary | Rapid Review | Open Access Journal

Received September 20, 2019, accepted October 19, 2019, date of publication October 24, 2019,
date of current version December 27, 2019.

Digital Object Identifier 10.1109/ACCESS.2019.2949423

Multi-Objective Machining Parameters Optimization for Chatter-Free Milling Process Considering Material Removal Rate and Surface Location Error

CONGYING DENG[1,3], YI FENG[1], JIANGUO MIAO[2], YING MA[1], AND BO WEI[1]
[1]School of Advanced Manufacturing Engineering, Chongqing University of Posts and Telecommunications, Chongqing 400065, China
[2]School of Aeronautics and Astronautics, Sichuan University, Chengdu 610065, China
[3]College of Mechanical Engineering, Chongqing University, Chongqing 400030, China

Corresponding author: Jianguo Miao (jianguomiao1992@163.com)

This work was supported in part by the National Natural Science Foundation of China under Grant 51705058, in part by the Chongqing Research Program of Basic Research and Frontier Technology under Grant cstc2017jcyjAX0005, in part by the China Postdoctoral Science Foundation Funded Project under Grant 2018M633314, and in part by the Chongqing Special Postdoctoral Science Foundation under Grant XmT2018040.

ABSTRACT In machining parameters optimization of a chatter-free milling process, the inevitable surface location error (SLE) reflecting the machined workpiece dimension accuracy has been barely considered as one objective representing the machining quality, lowering the optimization accuracy. Therefore, this paper provides an approach to establish a multi-objective optimization model, where the material removal rate (MRR) represents the machining efficiency and the SLE predicted in time-domain represents the machining quality. The non-dominated sorting genetic algorithm (NSGA-II) method is used to solve the multi-objective model and provide pareto optimal solutions to first determine some ideal optimal solutions. Then the analytic hierarchy process (AHP) and grey target decision (GTD) methods are combined to select one most satisfactory optimal solution which has a well balance between the MRR and SLE. A multi-objective model was established and taken as a case study to maximize the MRR and minimize the SLE. Comparison study was performed on this multi-objective model and two other mono-objective models for obtaining the optimal MRR and SLE respectively, which was combined with the influences of machining parameters on SLE to show the necessity of conducting a multi-objective optimization. Milling tests were conducted based on the solved optimal machining parameters, and the well consistence between the measured and predicted SLEs shows that the proposed multi-objective optimization method can provide an effective approach to balance the machining efficiency and quality when there are conflicts between different objectives.

INDEX TERMS Machining parameters optimization, multi-objective optimization model, surface location error, NSGA-II.

I. INTRODUCTION

The numerical control machining applied in the production of modern industry is essentially a process for removing the workpiece materials. Accordingly, improving the machining efficiency and obtaining higher workpiece quality has attained significant attentions in recent years [1]–[3]. The machining efficiency and quality are highly dependent on the machining parameters, e.g. the spindle speed, axial cutting depth, radial cutting width and feed rate per tooth. These machining parameters are critical factors to determine whether the chatter caused by the self-excited vibration will occur in the machining process. The chatter vibrations can lead to large forces, displacements, and poor surface quality. Then, the prerequisite to achieve higher machining efficiency and quality is that the machining process should be under chatter-free conditions. Generally, the chatter occurrence can be avoided by selecting appropriate machining parameters from stability lobe diagrams (SLDs) [4], [5]. Thus, an optimization analysis under stable constraints plays an important

The associate editor coordinating the review of this manuscript and approving it for publication was Shunfeng Cheng.

role for a machinist to obtain an optimal combination of machining parameters. However, during stable machining, the existing forced vibrations will also cause surface location errors and decrease workpiece geometric inaccuracies for the dynamic displacements of the tool. Therefore, extensive researches have been carried out to establish and solve the machining parameters optimization models [6]–[8].

Machining process efficiency is mainly focused on the time consumption and presented by the material removal rate (MRR). The MRR is usually taken as an objective in the machining parameter optimization. Budak et at. [9] proposed a method to obtain an optimal combination of axial cutting depth and radial cutting width which could maximize the chatter-free MRR. Since the optimization only considered the productivity and stable constraint, the part quality and equipment life cannot be guaranteed. Then the MRR is combined with other objectives (e.g. surface roughness, tool life, and cutting forces) to establish a multi-objective optimization model [10]–[12]. Sahu and Andhare [13] proposed a multi-objective optimization method considering the power consumption, material removal rate, surface roughness and tool wear in high speed milling, and combined the response surface methodology and genetic algorithm to select optimal machining parameters. Mia *et al.* [14] developed the machining parameters optimization for surface roughness, tool wear and material removal rate based on the Taguchi signal-to-noise ratio method. Furthermore, the MRR is applied to the field of green and high efficiency milling. Li *et al.* [15] used the MRR to represent the objective defined as specific energy consumption (SEC), and then a multi-objective optimization model was proposed and solved by the adaptive multi-objective particle swarm optimization algorithm for maximizing the energy efficiency and minimizing the production cost.

Various objective functions have been discussed in the researches about machining parameters optimization. However, the objective functions reflecting the machining quality have been addressed little. The surface roughness has been already used in representing the machining quality, but it is manly considered as one constraint and expressed based on empirical formulas and approximate models [16], [17]. Additionally, another important machining quality index named surface location error (SLE) has still not attained much attention in the machining parameters optimization [18]. The SLE is an inevitable phenomenon due to the forced vibration in a chatter-free machining process, which expresses the differences between the commanded and actual workpiece dimensions [19], [20]. Researches have been already developed on the SLE. For instance, Schmitz's team proposed methods to predict the SLE in time and frequency domain, and pointed out that the SLE was dependent on the machining parameters [21], [22]. As the SLE determines the geometric accuracy of the workpiece, it should be discussed in the machining parameters optimization [23]. Zhang et al. [24] had emphasized uncertain parameters in milling process and established a formulation for obtaining the robust minimum SLE and maximum spindle speed. The optimization was solved by an augmented Lagrangian function method, but only considering the spindle speed cannot guarantee the optimal machining efficiency.

Given the lack of surface location error application in machining parameters optimization, the MRR and SLE are designed as the objectives in this paper to establish a multi-objective optimization model for obtaining an optimal machining parameters combination, which can realize a well balance between the milling efficiency and quality. Formulas for calculating the SLE are derived based on the machined surface geometry predicted by the cycloidal tool path time-domain simulation. Then the non-dominated sorting genetic algorithm with elitist strategy (NSGA-II) is proposed to find the pareto optimal solutions of the multi-objective optimization model. And the analytic hierarchy process (AHP) and grey target decision (GTD) methods are further combined to select one most satisfactory optimal solution from the pareto optimal solutions.

The rest of this paper is organized as follows. Section II describes the SLE caused by forced vibrations during a stable machining process and presents an algorithm for predicting the SLE in time domain. Section III provides detailed information and procedures of establishing a multi-objective optimization model for improving the machining efficiency and quality. How to obtain the most satisfactory optimal solution of the proposed multi-objective optimization model based on NSGA-II, AHP and GTD methods is presented in section IV. Section V describes the multi-objective optimization on a CNC machine tool and validates its feasibility by milling experiments. Finally, conclusions are reached in section VI.

II. SLE ALGORITHM IN TIME DOMAIN

During stable milling, the tool experiences the forced vibrations which depend on the system dynamic parameters, process parameters and tool path frequency. The dynamic displacements of the tool result an undercut or overcut condition of the workpiece surface. A visual description of a SLE phenomenon under the overcut case is shown in Fig. 1, where more materials are removed than commanded for down milling. In this section, a time-domain simulation for the SLE predication is detailed in two basic steps. First, the cutting forces in x and y directions, $F(t)$, are expressed in time-domain based on instantaneous chip thickness. Second, the tool vibration displacements in x and y directions, Dv(t), are calculated using numerical integration method and the coordinate values are finally sampled at the exit for down milling or cut entry for up milling to determine the SLE.

A. TIME-DEPENDENT FORCE CALCULATION

A standard two degree of freedom dynamic model for a milling process is described in Fig. 1. The tool is assumed to be compliant relative to the rigid workpiece. Cutting forces

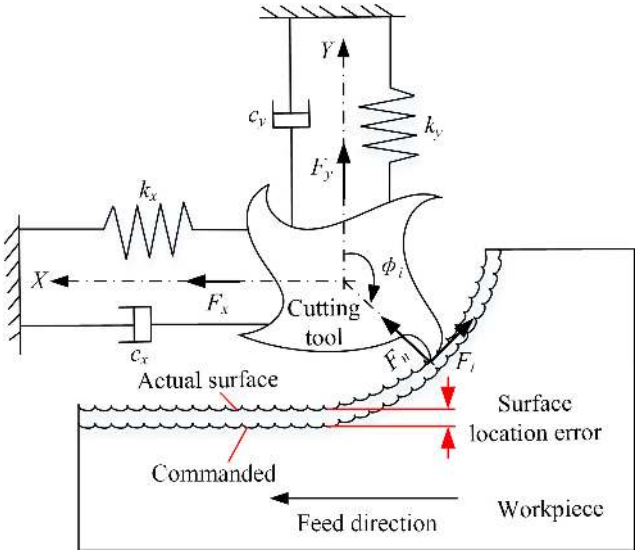

FIGURE 1. Two degree of freedom dynamic model for milling system and an example of an undercut condition.

in x and y directions (F_x and F_y) are expressed as:

$$\begin{aligned} F_x &= \sum_{i=1}^{N_t} F_t \cos(\phi_i) + F_n \sin(\phi_i) \\ &= \sum_{i=1}^{N_t} K_t a_p h(\phi_i) \cos(\phi_i) + K_n a_p h(\phi_i) \sin(\phi_i) \\ F_y &= \sum_{i=1}^{N_t} F_t \sin(\phi_i) - K_n \cos(\phi_i) \\ &= \sum_{i=1}^{N_t} K_t a_p h(\phi_i) \sin(\phi_i) - K_n a_p h(\phi_i) \cos(\phi_i) \end{aligned} \quad (1)$$

where F_t and F_n are the tangential and normal cutting forces, a_p is the axial cutting depth, $h(\phi_i)$ is the instantaneous chip thickness determined by the feed rate per tooth f_t and written as $h(\phi_i) = f_t * \sin(\phi_i)$, ϕ_i is the i_{th} tooth angle dependent on spindle speed, N_t is the number of tooth, and K_t and K_n are the tangential and normal cutting force coefficients respectively. Considering the vibrations in real milling process, the instantaneous chip thickness $h(\phi_i)$ should be uploaded as:

$$h(\phi_i) = f_t \sin(\phi_i) + n(t-\tau) - n \quad (2)$$

Where $\tau = 60/N_t\Omega$ is the tooth period and Ω is the spindle speed; and n represents the tool vibration in the normal direction that can be described as:

$$n = x \sin(\phi_i) - y \cos(\phi_i) \quad (3)$$

The above equations show that the cutting forces are a function of time or tooth angle. Thus, to have a convenient calculation, the tooth angle is divided into a discrete number of steps. At each small time step dt, the tooth angle is increased by a corresponding small angle dϕ. As the tool experiences the rotary motion, dϕ and dt are determined by the number of steps per revolution labeled as N_r, $\mathrm{d}\phi = 360/N_r$ (deg) and $\mathrm{d}t = 60/N_r\Omega$ (s). This discretion benefits storing the surface information created by the previous tooth at each angle, and then the current chip thickness can be calculated using Eq. (3). And the approach to obtain the vibration displacements in x and y directions are discussed in the following section *B*.

Generally, the cutting edges are inclined at a helix angle β, and this geometry results in that the full length of the cutting edge does not enter or exit the cut at the same instant. Therefore, a cutting edge is discretized into a number of slices along the z direction to consider the delay condition. The thickness of each slice along the axial cutting depth a_p is defined as Δb, and then the angular delay $\Delta\phi$ between two slices is:

$$\Delta\phi = 2\Delta b \tan(\beta)/D \quad (4)$$

where D is the tooth diameter. Then at a specific time T_s, the cutting forces expressed in Eq. (1) is updated:

$$\begin{aligned} F_x &= \sum_{i=1}^{N_t}\sum_{j=1}^{N_m} g(\phi_{ij}) \left(K_t \Delta b h(\phi_{ij}) \cos(\phi_{ij}) \right. \\ &\quad \left. + K_n \Delta b h(\phi_{ij}) \sin(\phi_{ij})\right) \\ F_y &= \sum_{i=1}^{N_t}\sum_{j=1}^{N_m} g(\phi_{ij}) \left(K_t \Delta b h(\phi_{ij}) \sin(\phi_{ij}) \right. \\ &\quad \left. - K_n \Delta b h(\phi_{ij}) \cos(\phi_{ij})\right) \\ \phi_{ij} &= (T_s \bmod \mathrm{d}t) - i\frac{N_r}{N_t} - j\Delta\phi \end{aligned} \quad (5)$$

where ϕ_{ij} is the current angle for the j_{th} slice of the i_{th} tooth, and $g(\phi_{ij})$ is the function defining whether the current slice engages a cut. If the slice angle is between the cut entry and exit angles, $g(\phi_{ij})$ equals 1; otherwise, $g(\phi_{ij})$ equals 0. Therefore, the time-dependent cutting forces can be calculated using Eq. (5).

B. DISPLACEMENT AND SLE CALCULATION

According to Fig.1, the motion equation of the milling system in x and y directions are:

$$F_x = m_x\ddot{x} + c_x\dot{x} + k_x x \text{ and } F_y = m_y\ddot{y} + c_y\dot{y} + k_y y \quad (6)$$

where m, c and k are the modal mass, modal damping and modal stiffness respectively, and the subscripts represent x and y directions. Specific values of these modal parameters are typically obtained from the impact testing followed by a modal fitting technique. If there are more than one dominant mode in each direction, the modal superposition method is applied to fascinate the displacements calculation.

Equation (6) is rewritten for obtaining the accelerations in x and y directions at the current time step:

$$\ddot{x} = \frac{F_x - c_x\dot{x} - k_x x}{m_x} \text{ and } \ddot{y} = \frac{F_y - c_y\dot{y} - k_y y}{m_y} \quad (7)$$

where velocities, $\dot{x}$ and $\dot{y}$, and displacements, x and y, are the values of the previous time step. To carry out the simulation,

the initial values are set zero. Then a numerical integration is adopted to compute the new velocities and displacements:

$$\dot{x} = \dot{x} + \ddot{x} \cdot dt \text{ and } \dot{y} = \dot{y} + \ddot{y} \cdot dt \tag{8}$$

$$x = x + \dot{x} \cdot dt \text{ and } y = y + \dot{y} \cdot dt \tag{9}$$

where the velocities in the right side of the equation are the values of the previous time step. The calculated new velocities are further used to compute the new displacements in Eq. (9). Similarly, the vibration displacements in the right side of the equation are the values of the previous time step.

The calculated displacements at the current time step are stored and used to obtain the instantaneous chip thickness for the next time step based on Eqs. (2) and (3). Then the cutting forces are updated using Eq. (5) and further used to calculate the new displacements. At each iteration, the new vibration displacements are used to obtain the coordinate values of the current surface point based on the following Eq. (10) (assuming that the nominal coordinate of tool center is 0):

$$\begin{aligned} s_x &= \frac{D}{2}\sin\left(\phi_{ij}\right) + \frac{N_t f_t}{N_r} + x \\ s_y &= \frac{D}{2}\cos(\phi_{ij}) + y \end{aligned} \tag{10}$$

With the final coordinate vectors in x and y directions, a trimming algorithm is adopted to identify the extreme points on the tool path and define the machined surface geometry (an example is displayed in Fig. 2). First, the points with the coordinate values meeting the following condition are selected:

$$\begin{aligned} S_y &< -Q_c * \frac{D}{2} \text{ down milling} \\ S_y &> Q_c * \frac{D}{2} \text{ up miling} \end{aligned} \tag{11}$$

where Q_c is an appropriately defined coefficient, such as 0.95. The selected points are arranged on the tool path in the ascending x-feed direction. Values of these points are compared repeatedly to keep the lower ones for down milling or the higher ones for up milling, determining the final machined surface geometry. Then the surface location error is calculated using the mean value of the final selected points ($S_{average}$) and the tool diameter D:

$$\begin{aligned} \text{SLE} &= \left(\frac{D}{2} + S_{average}\right) \text{ down milling} \\ \text{SLE} &= -\left(\frac{D}{2} - S_{average}\right) \text{ up miling} \end{aligned} \tag{12}$$

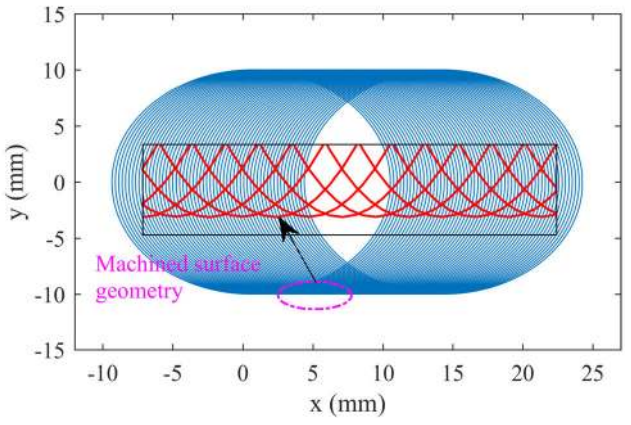

FIGURE 2. An example of the final tool path and machined surface geometry.

III. MULTI-OBJECTIVE OPTIMIZATION MODEL OF A MILLING PROCESS

Selecting the optimal machining parameters is an important strategy for manufacturers to improve the machining efficiency and quality. Researchers have discovered that effects of the machining parameters on the efficiency and quality are mainly opposite. For instance, a higher axial cutting depths increases MRR, but a chatter vibration can occur and worsen the machined surface quality. Since a multi-objective optimization emphasizes the importance of all objectives, it is applicable for finding a satisfactory result to balance the machining efficiency and quality. Thus, this section discusses the variables, objectives and constraints to establish a multi-objective optimization model.

A. VARIABLES

The stability is a prerequisite for a milling process, and an appropriate combination of spindle speed Ω, axial cutting depth a_p, radial cutting width a_e and feed rate per tooth f_t are the main approach to avoid the chatter occurrence. Moreover, these machining parameters are the main factors affecting the machining efficiency and quality. Accordingly, the spindle speed Ω, axial cutting depth a_p, radial cutting width a_e and feed rate per tooth f_t are determined as the variables, and their variation ranges are detailed in the following section C.

B. OBJECTIVE FUNCTION

Many researches have been developed on the objective functions to represent the machining efficiency and part quality to optimize the machining parameters, such as the material removal rate, energy consumption, surface roughness and so on. In this paper, the frequently-used material remove rate MRR is adopted to express the machining efficiency, and the rarely discussed surface location error SLE is adopted to express the part quality.

1) MATERIAL REMOVAL RATE

Material removal rate refers to the volume of metal material removed by the tool per unit time, and it is a product of the spindle speed Ω, axial cutting depth a_p, radial cutting width a_e and feed rate per tooth f_t. The MRR is expressed as follow:

$$MRR = \frac{\Omega * a_p * a_e * f_t * N_t}{60} \tag{13}$$

where N_t is the number of tooth. Equation (13) shows that the MRR (mm^3/s) is a linear function of the variables, and an increment of any variable can increase the MRR.

2) SURFACE LOCATION ERROR

The surface location error refers to the difference between the commanded and machined surface, which can affect the geometric dimension accuracy of workpiece. The equations to compute the SLE have been discussed in section II, and it can be seen from those equations that the SLE is an implicit function of the variables (Ω, a_p, a_e and f_t,) and not directly proportional to each variable. Furthermore, since the SLE can have a positive or negative values for different machining process with different machining parameters, its absolute value is defined as the final optimization objective.

C. CONSTRAINTS

In a real milling process, the selection of machining parameters is also subject to the performance of the machine tool and cutting tool, i.e. cutting power, tool life and cutting force. Therefore, the optimization should be developed under the following constraints.

1) VALUE RANGES OF THE VARIABLES

Values of the machining parameters must vary within specific ranges which are recommended by the experienced technologist, tool manufacturer, workpiece dimension, process requirements and so on [25].

$$\begin{cases} \Omega_{\min} < \Omega < \Omega_{\max} \\ a_{p\min} < a_p < a_{p\max} \text{ and } a_{p\max} < a_{p\lim} \\ a_{e\min} < a_e < a_{e\max} \\ f_{t\min} < f_t < f_{t\max} \end{cases} \tag{14}$$

where the variables with subscripts labeled as min and max mean the minimum and maximum values, and the $a_{p\lim}$ means the limiting axial cutting depth. The $a_{p\max}$ must be less than the $a_{p\lim}$ to avoid chatter occurrence in the milling process, and the $a_{p\lim}$ is typically obtained from the milling stability analysis proposed by Altintas [26].

2) POWER CONSTRAINT

The needed power should be less than the power output of the machine tool.

$$P_{actual} = \frac{F * \Omega * \pi}{60000\eta} \le P_{m\max} \tag{15}$$

where η is the machining tool efficiency coefficient, F is the cutting force, and $P_{m\max}$ is the maximum power.

3) SURFACE ROUGHNESS CONSTRAINT

The surface roughness is another index reflecting surface quality, and it should be smaller than the required one. The surface roughness can be calculated based on the equations to calculate the SLE, and it can be expressed as follow.

$$R_a = \frac{\sum_{l=1}^{n_p} \left| S_{yl} - S_{average} \right|}{n_p} \tag{16}$$

where R_a is the surface roughness, n_p is the number of the final selected surface points in section II, S_{yl} is the coordinate of l_{th} final selected point, and $S_{average}$ is the mean value.

4) TOOL LIFE CONSTRAINT

The tool life are considered to ensure an economy machining process. The tool life is generally calculated using Eq. (17), and it should be longer than the one proposed by technologists.

$$T_{tool} = \frac{C_v^{1/q} D^{a/q}}{v_c^{1/q} f_t^{d/q} a_p^{e/q} a_e^{g/q} N_t^{w/q}} \tag{17}$$

where $v_c = \pi * D * \Omega/60$ is the cutting velocity, v_c, and C_v, a, d, e, g, w and q are the coefficients can be obtain from the CNC machining manual.

D. OPTIMIZATION MODEL

Based on the defined variables, objectives and constraints, the multi-objective optimization model of a milling process is formulated as follows for maximizing the machining efficiency and minimizing the surface location error.

$$\begin{aligned} &\min f(U) = \left(\min(-\text{MRR}),\ \min(|\text{SLE}|) \right) \\ &U = \left(\Omega\ a_p\ a_e\ f_t \right)^T \\ &s.t. \begin{cases} U_{\min} \le U_{\max} \\ P \le \eta P_{\max} \\ R_a \le R_{a\min} \\ T_{actual} \le T_{tool} \end{cases} \end{aligned} \tag{18}$$

IV. OPTIMIZATION SOLUTION VIA NSGA-II ALGORITHM

The results solved from the multi-objective optimization model should satisfy the requirements of each objective simultaneously. Generally, there are wo methods used to solve the multi-objectives optimization model. One method uses an weighted-sum approach for assigning a certain weight to each objective, and then transforms the multi-objective optimization into a single objective optimization [27], [28]. However, these objectives have different dimensions and there is no uniform criterion to assign the weight of each objective appropriately, resulting in decrease of the optimization accuracy. Considering this problem, a number of multi-objective optimization algorithms are proposed based on evolutionary technique [29]–[31]. The non-dominant sorting genetic algorithm with elite strategy (NSGA-II) has demonstrated its greater efficiency, stability and accuracy in obtaining the pareto optimal solutions [32], [33]. NSGA-II reduces the computational complexity, proposes the concept of crowding degree to diversify the population, and introduces the elite strategy to expand the sample range. Due to the features of the NSGA-II, it is used to solve the multi-objective optimization model in this research.

A. BASIC LOGIC STRUCTURE OF NSGA-II

The flow chart of the NSGA-II is shown in Fig.3(a). First, number of the parent population P_P is determined as N_p

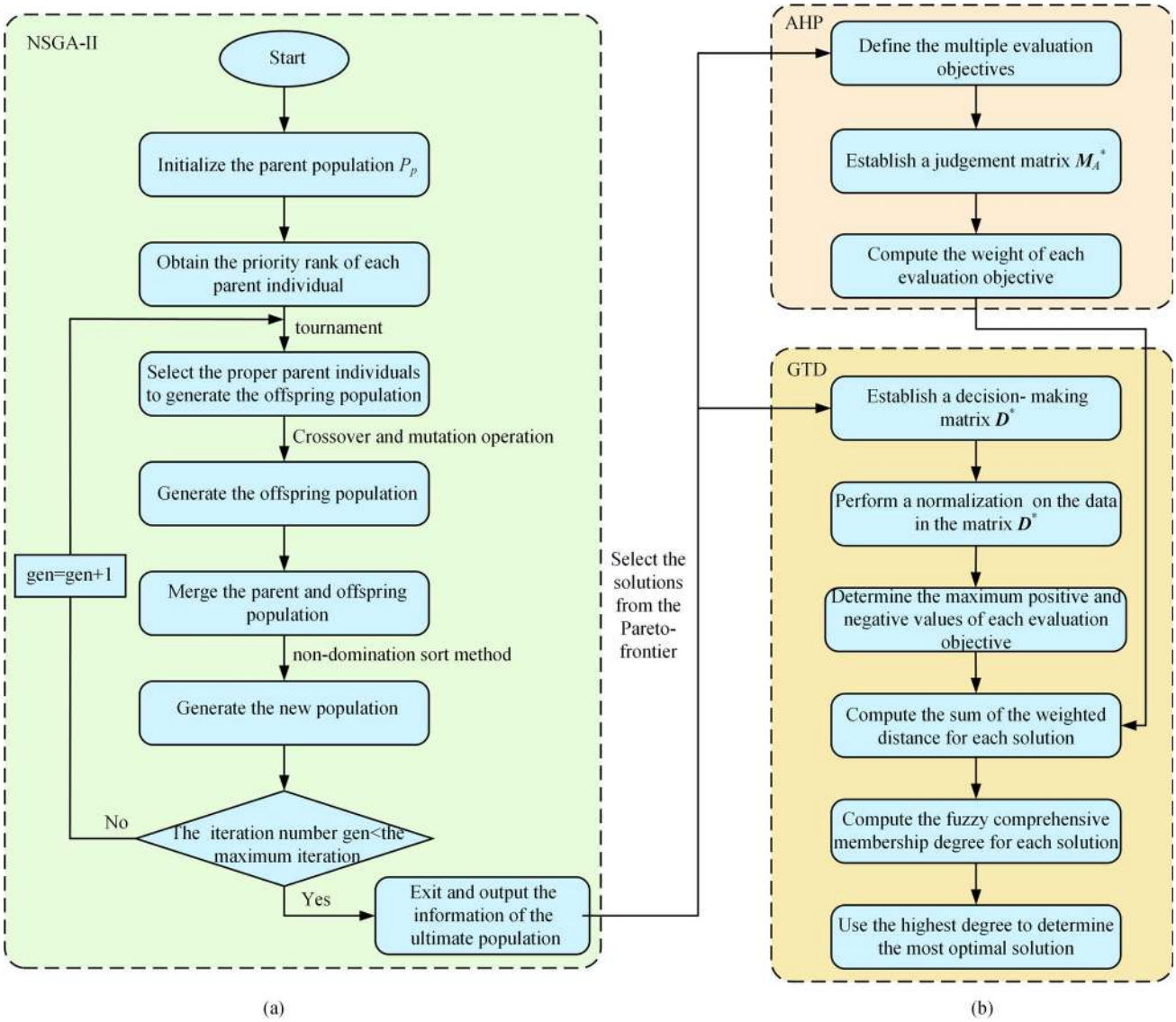

FIGURE 3. (a) The flow charts of the NSGA-II method. (b) The flow chart of the AHP and GTD methods.

and each individual is formed by the values of all variables. The values of each parent individual are initialized randomly within the defined variation range. The objective values of each individual are calculated based on the objective functions, and compared using the non-dominant sorting method to obtain the priority rank. For the individuals with the same rank, their crowding distances are calculated to further identify the priority. The parent individuals with higher priority rank and crowding degree are selected to generate the offspring P_o based on the crossover and mutation operations. Then the parent population P_P and the offspring population P_o are combined to compute the priority ranks, and the top N_p individuals are retained to form a new population P_{new}. The new population P_{new} is used to repeat the above procedures until the termination condition is satisfactory.

For the non-dominant sorting method, the calculated objective values more closer to the requirements are defined to be dominant. During the sorting process, the objective values of one individual are compared with those of the others, and then the dominance between two individuals can be determined. Q is the number of one individual dominated by others, and $\boldsymbol{S}_Q$ is the vector recoding the individuals dominated by this individual. If Q equals 0, the non-dominant rank number of the individual is defined as one. Then, the Q value of each element in the vector $\boldsymbol{S}_Q$ minuses 1. If the new Q value of one individual equals 0, the corresponding non-dominant rank number is defined as two. Therefore, repeating this process, the non-dominant rank of each individual can be obtained.

The individual with a lower rank number is a better solution for the optimization. If the non-dominant rank numbers of the individuals are the same, the individual with a larger

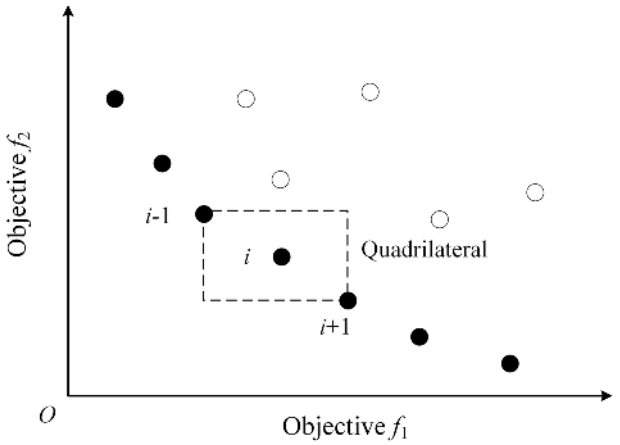

FIGURE 4. The crowding distances of the individuals.

crowding distance is first selected. The crowding distance shown in Fig. 4 is the sum of the length and width of the quadrilateral, and it can be calculated using the following equation:

$$Dis\,(i) = \sum_{j=1}^{m} \left(\left| O^{j}_{vi+1} - O^{j}_{vi-1} \right| \right) \tag{19}$$

where $Dis(i)$ is the crowding distance of the i_{th} individual, m is the number of the objectives, and O^{j}_{vi+1} and O^{j}_{vi-1} are the j_{th} objective values of the $i{+}1_{th}$ and i-1_{th} individuals. Individuals with large crowding distances benefit the diversity of the population as they have more opportunities to participate in the reproduction and evolution.

B. SELECTION OF THE OPTIMAL SOLUTION BASED ON THE AHP AND GTD METHODS

The NSGA-II method only provides a Pareto-optimal front for the multi-objective optimization model. Then the analytic hierarchy process AHP and grey target decision GTD methods are combined to select a most satisfactory solution from the Pareto-optimal front to balance the objectives in this paper [34], [35]. A flow chart for expressing the selection based on the AHP and GTD methods is presented in Fig.3(b).

1) THE ANALYTIC HIERARCHY PROCESS METHOD

The AHP method is a measurement theory for decision-making based on the combination of the qualitative and quantitative analyses, which has been widely used in various multi-objective decision-making researches. The AHP method allows the experts to judge the dominance of one element over another through pairwise comparisons, and then a decision matrix can be constructed to compute the weight of each element for benefiting the optimal scheme selection. The specific application of the AHP method is illustrated in the following two steps.

The first step is defining the multiple evaluation objectives for the decision-making and using the 1-9 scaling method to represent the result of each pairwise comparison of the evaluation objectives. Then a judgement matrix M^{*}_{A} shown in Eq. (20) can be established, and the corresponding relationships between the numbers and the dominances are expressed in Table 1.

TABLE 1. The scaling numbers and the corresponding meanings.

Comparation	Scaling number	Meaning
Factor A compares to factor B	1	A and B are equally important
	3	A is slightly more important than B
	5	A is much more important than B
	7	A is strongly more important than B
	9	A is extremely more important than B
	2 4 6 8	Intermediate results of the above adjacent judgments
	Reciprocals of these numbers	Opposite results of the above judgments

$$\boldsymbol{M}^{*}_{A} = \begin{bmatrix} & M_1 & \cdots & M_{i-1} & M_i & M_{i+1} & \cdots & M_n \\ M_1 & f_{11} & \cdots & f_{1i-1} & f_{1i} & f_{1i+1} & \cdots & f_{1n} \\ \vdots & \vdots & \vdots & \vdots & \vdots & \vdots & \vdots & \vdots \\ M_{i-1} & f_{i-11} & \cdots & f_{i-1i-1} & f_{i-1i} & f_{i-1i+1} & \cdots & f_{i-1n} \\ M_i & f_{i1} & \cdots & f_{ii-1} & f_{ii} & f_{i1+1} & \cdots & f_{in} \\ M_{i+1} & f_{i+11} & \cdots & f_{i+1i-1} & f_{i+1i} & f_{i+1i+1} & \cdots & f_{i+1n} \\ \vdots & \vdots & \vdots & \vdots & \vdots & \vdots & \vdots & \vdots \\ M_n & f_{n1} & \cdots & f_{ni-1} & f_{ni} & f_{ni+1} & \cdots & f_{nn} \end{bmatrix} \tag{20}$$

where n is the total number of the evaluation objectives, M_i is the i_{th} evaluation objective, f_{in} is the comparison result between the i_{th} objective and the n_{th} objective, the comparison result is an integer between 0 and 9, and the values of the elements on the diagonal all equal 1.

The second step is computing the weight vector for the evaluation objectives based on the following equation:

$$\boldsymbol{M}^{*}_{A}\boldsymbol{W} = \lambda \boldsymbol{W} \tag{21}$$

where λ is the max real eigenvalue satisfying the equation, and $\boldsymbol{W}$ is the eigenvector corresponding to the maximum positive eigenvalue. The eigenvector or the weight vector $\boldsymbol{W}$ has the following form:

$$\boldsymbol{W} = \left[W_1 \cdots W_{i-1}\ W_i\ W_{i+1} \cdots W_n \right] \tag{22}$$

where W_i is the weight for the i_{th} evaluation objective.

2) THE GREY TARGET DESIGN METHOD

The application of the GTD method often contains the following four steps.

The first step is utilizing the specific values of the defined evaluation objectives to form a decision-making matrix $\boldsymbol{D}^{*}$, and the specific values can be obtained from the information of the Pareto optimal solutions. The matrix $\boldsymbol{D}*$ is shown in Eq. (23), and the most satisfactory solution is selected from

the matrix $\boldsymbol{D}^*$.

$$\boldsymbol{D}^* = \begin{bmatrix} \boldsymbol{D}_1 \\ \vdots \\ \boldsymbol{D}_{i-1} \\ \boldsymbol{D}_i \\ \boldsymbol{D}_{i+1} \\ \vdots \\ \boldsymbol{D}_m \end{bmatrix} = \begin{bmatrix} d_{11} & \cdots & d_{1i-1} & d_{1i} & d_{1i+1} & \cdots & d_{1n} \\ \vdots & \vdots & \vdots & \vdots & \vdots & \vdots & \vdots \\ d_{j-11} & \cdots & d_{j-1i-1} & d_{j-1i} & d_{j-1i+1} & \cdots & d_{j-1n} \\ d_{j1} & \cdots & d_{ji-1} & d_{ji} & d_{ji+1} & \cdots & d_{jn} \\ d_{j+11} & \cdots & d_{j+1i-1} & d_{j+1i} & d_{j+1i+1} & \cdots & d_{j+1n} \\ \vdots & \vdots & \vdots & \vdots & \vdots & \vdots & \vdots \\ d_{m1} & \cdots & d_{mi-1} & d_{mi} & d_{mi-1} & \cdots & d_{mn} \end{bmatrix} \quad (23)$$

where $\boldsymbol{D}_i$ means the i_{th} solution, m is the number of the solutions, d_{ji} is the specific value of the i_{th} evaluation objective in the j_{th} solution.

As the evaluation objectives often have different meanings and units, the second step is normalizing values of the evaluation objectives between -1 and 1 to eliminate the influences caused by the physical dimensions. The normalization is performed based on the following equations:

$$r_{ji} = \frac{d_{ji} - z_i}{\max\left(\max\limits_{1\le j\le m}\{d_{ji}\} - z_i, z_i - \min\limits_{1\le j\le m}\{d_{ji}\}\right)} \quad (24)$$

$$r_{ji} = \frac{z_i - d_{ji}}{\max\left(\max\limits_{1\le i\le n}\{d_{ji}\} - z_i, z_i - \min\limits_{1\le i\le n}\{d_{ji}\}\right)} \quad (25)$$

where r_{ji} is the normalized value of the i_{th} evaluation objective in the j_{th} solution, d_{ji} is the corresponding specific value in the Eq. (23), z_i is the mean value of the i_{th} evaluation objective. If a bigger d_{ji} can benefit the machining process, the Eq. (24) is used to perform the normalization; otherwise, the Eq. (25) is used to perform the normalization.

After the normalization, the original matrix $\boldsymbol{D}^* = (d_{ji})_{m\times n}$ is transformed into the matrix $\boldsymbol{R}^* = (r_{ji})_{m\times n}$ shown in Eq. (26), and the maximum positive and negative values of each evaluation objective are expressed in Eq. (27).

$$\boldsymbol{R}^* = \begin{bmatrix} \boldsymbol{R}_1 \cdots \boldsymbol{R}_{i-1} \ \boldsymbol{R}_i \ \boldsymbol{R}_{i+1} \cdots \boldsymbol{R}_n \end{bmatrix}^{\mathrm{T}} \quad (26)$$

$$r_i^{*+} = \max_{1\le j\le t_i}\{r_{ji}\}, \quad r_i^{*-} = \min_{1\le j\le m-t_i}\{r_{ji}\} \quad (27)$$

where t_i is the total number of the i_{th} evaluation objective with positive values, and r_i^{*+} and r_i^{*-} are the maximum positive value and the minimum negative value of the i_{th} evaluation objective respectively. The r_i^{*+} and r_i^{*-} are named the positive bull's-eye and the negative bull's-eye respectively. The solution with the positive bull's-eye of each evaluation objective is defined as the positive bull's-eye solution $\boldsymbol{R}^{*+}$, and the solution with the negative bull's-eye of each evaluation objective is defined as the negative bull's-eye solution $\boldsymbol{R}^{*-}$. The $\boldsymbol{R}^{*+}$ and $\boldsymbol{R}^{*-}$ have the following forms respectively:

$$\boldsymbol{R}^{*+} = \begin{bmatrix} r_1^{*+} \cdots r_{i-1}^{*+} \ r_i^{*+} \ r_{i+1}^{*+} \cdots r_n^{*+} \end{bmatrix} \quad (28)$$

$$\boldsymbol{R}^{*-} = \begin{bmatrix} r_1^{*-} \cdots r_{i-1}^{*-} \ r_i^{*-} \ r_{i+1}^{*-} \cdots r_n^{*-} \end{bmatrix} \quad (29)$$

In the third step, the sum of the weighted distance between each evaluation objective and the corresponding positive bull's-eye is defined as d_j^{*+}, and the sum of the weighted distance between each evaluation objective and the corresponding negative bull's-eye is defined as d_j^{*+}:

$$d_j^{*+} = \sqrt{\sum_{i=1}^{n} W_i \left(r_{ji} - r_i^{*+}\right)^2}, \ d_j^{*-} = \sqrt{\sum_{i=1}^{n} W_i \left(r_{ji} - r_i^{*-}\right)^2} \quad (30)$$

where W_i is the weight of the i_{th} evaluation objective shown in Eq. (22), d_j^{*+} describes the deviation between the i_{th} solution $\boldsymbol{R}_i$ and the positive bull's-eye solution $\boldsymbol{R}^{*+}$, and d_j^{*-} describes the deviation between the i_{th} solution $\boldsymbol{R}_i$ and the negative bull's-eye solution $\boldsymbol{R}^{*-}$.

In the fourth step, the deviations d_j^{*+} and d_j^{*-} are used to calculate the fuzzy comprehensive membership degree u_j of the j_{th} solution:

$$u_j = \left[1 + \left(d_j^{*+} \Big/ d_j^{*-}\right)\right]^{-1} \quad (31)$$

The bigger the u_j, the better the solution. Thus, after the fuzzy comprehensive membership degree of each solution is computed, these solutions can be sorted to determine the optimal one.

V. CASE STUDY AND RESULTS DISCUSSION

To better illustrate the application of the proposed multi-objective optimization method and validate its feasibility in real machining process, a case study that contains a simulation of the machining parameters optimization and a series of experiments has been performed on a CNC vertical machining center.

A. NSGA-II FOR MACHINING PARAMETERS OPTIMIZATION

The basic information of the CNC vertical machining center and machining parameters are presented in Table 2. The down milling is defined, the workpiece material is the common used 45 steel, the surface roughness R_a is defined no more than 3.2, the cemented carbide end milling cutter whose diameter is 20 mm with an overhang of 45 mm and four teeth is selected, the tangential cutting force coefficient K_t is 1428 MPa, the normal cutting force coefficient K_n is 826 MPa, the coefficients C_v, a, d, e, g, w and q to calculate the tool life are 284, 0.48, 0.37, 0.18, 0.34, 0.08 and 0.12, the required tool life is 60 min, and each machining parameter varies within its defined range listed in Table 2.

The multi-objective optimization model for obtaining the optimal combination of machining parameters is established

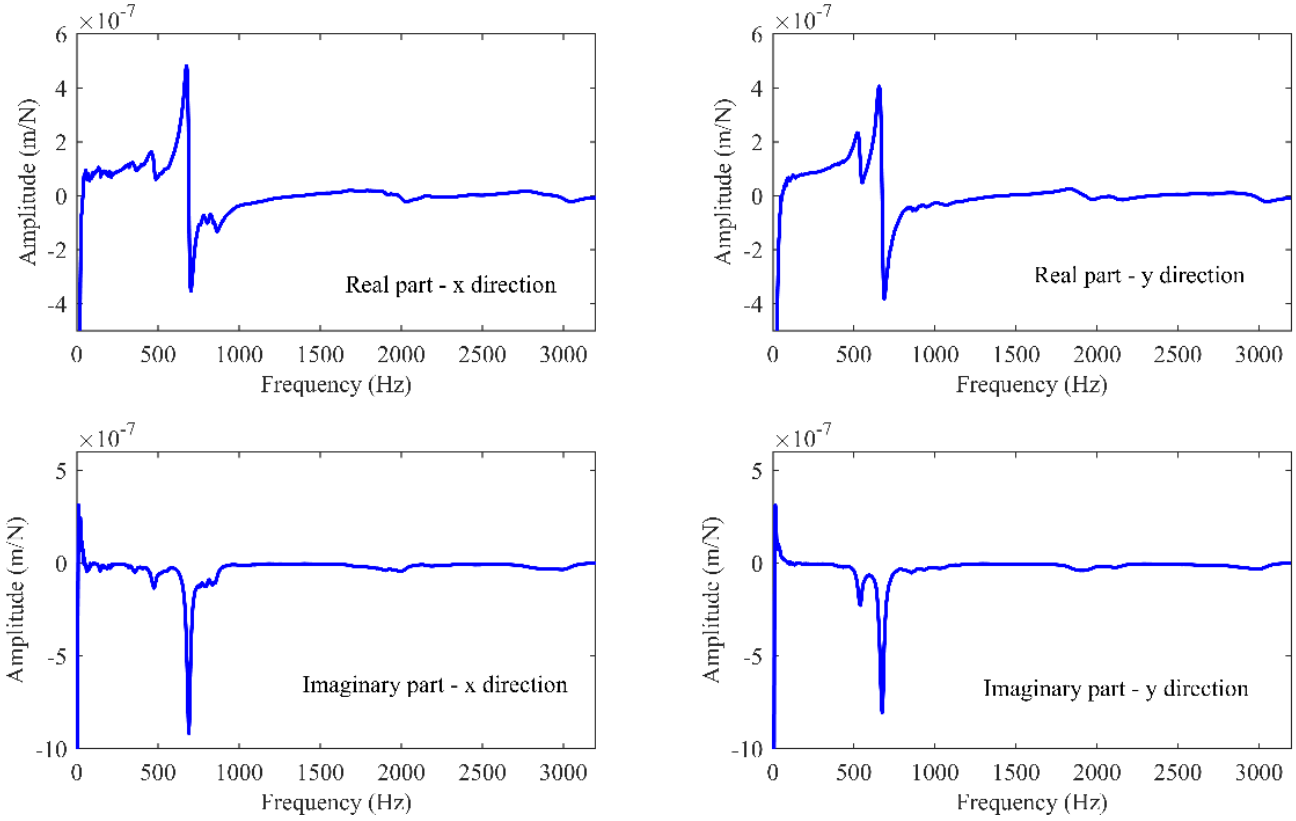

FIGURE 5. The measured tool tip FRFs in *x* and *y* directions.

TABLE 2. Information of the machine tool and the milling conditions.

Symbol	Unit	Numerical data
Power	$P_{\max}$ (Kw)	7.5
Power coefficient	η	0.8
Spindle speed	$[\Omega_{\min}, \Omega_{\max}]$ (rpm)	[2500, 10000]
Axial cutting depth	$[a_{p\min}, a_{p\max}]$ (mm)	[0.02, 15]
Radial cutting width	$[a_{e\min}, a_{e\max}]$ (mm)	[0.02, 20]
Feed rate per tooth	$[f_{t\min}, f_{t\max}]$ (mm/z)	[0.02, 0.2]

and solved based on the proposed NSGA-II, AHP and GTD methods in the environment of Matlab software. The required basic parameters for the multi-objective optimization are set as follows: the initial population size is 80, the iteration number is 100, the crossover probability is 0.8, and the mutation probability is 0.05. Before the optimization, the impact testing was performed on the tool tip to measure the frequency response functions (FRFs) shown in Fig. 5 and identify the related modal parameters by the modal fitting technique.

B. THE RESULTS AND DISCUSSIONS OF THE NSGA- II OPTIMIZATION

After the optimization, the finally obtained Pareto-optimal front is shown in Fig. 6. The variation tendency of the solutions in the Pareto-optimal front are divided into three sections: in section AB, the material removal rate and absolute surface location error both have smaller values; in the section

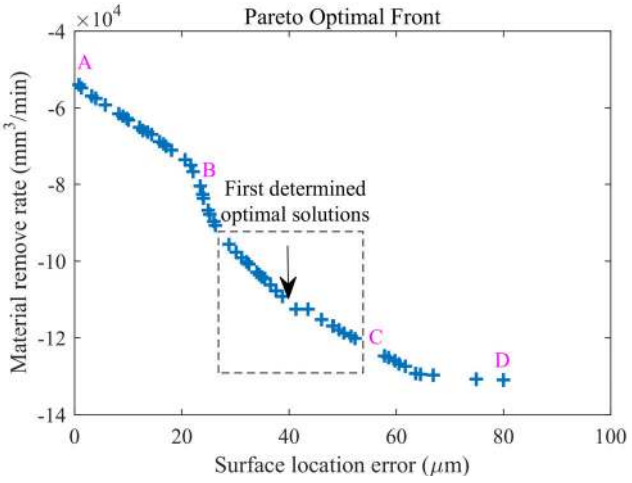

FIGURE 6. The Pareto-optimal front of the multi-objectives optimization.

CD, as the absolute surface location increases, the material removal rate barely increases; and in the section BC, the material removal rate and absolute surface location error have appropriate values, and the variation ratio of the material removal rate is much higher than that of the absolute surface location error. Therefore, some solutions in the section BC are first determined as the initial optimal solutions. The corresponding machining parameters and the objectives of the initial optimal solutions are described in Table 3. Then

TABLE 3. The information of the determined initial optimal solutions.

Order	Spindle speed (rpm)	Cutting depth (mm)		Feed rate per tooth (mm/per)	Surface location error (μm)	Materials removal rate (10^5mm^3/min)	Tool life (min)	Fuzzy comprehensive membership degree u	Sort
		Axial	Radial						
1	3387	6.35	5.56	0.20	28.83	0.96	86.72	0.580	8
2	3387	6.44	5.60	0.20	30.13	0.98	86.16	0.602	7
3	3385	6.49	5.64	0.20	31.12	0.99	85.85	0.610	6
4	3378	6.53	5.68	0.20	32.07	1.00	85.92	0.656	2
5	3379	6.56	5.69	0.20	32.56	1.01	85.70	0.676	1
6	3385	6.61	5.75	0.20	34.02	1.03	84.71	0.652	3
7	3385	6.63	5.76	0.20	34.43	1.03	84.59	0.625	4
8	3394	6.54	5.86	0.20	34.90	1.04	83.53	0.542	10
9	3383	6.62	5.83	0.20	35.54	1.04	84.25	0.622	5
10	3394	6.57	5.95	0.20	36.47	1.06	82.83	0.536	11
11	3397	6.66	5.95	0.20	37.58	1.08	82.39	0.553	9
12	3408	6.61	6.05	0.20	38.71	1.09	81.14	0.393	20
13	3408	6.78	6.08	0.20	41.31	1.12	80.51	0.400	19
14	3389	7.02	5.91	0.20	43.48	1.12	82.25	0.504	12
15	3389	7.02	6.05	0.20	46.00	1.15	81.31	0.489	14
16	3388	7.13	6.04	0.20	48.07	1.17	81.17	0.494	13
17	3389	7.14	6.04	0.20	48.30	1.17	81.08	0.475	16
18	3388	7.15	6.08	0.20	49.29	1.18	80.86	0.476	15
19	3389	7.12	6.15	0.20	50.20	1.19	80.42	0.462	17
20	3389	7.22	6.11	0.20	51.50	1.20	80.43	0.459	18

the AHP and GTD methods are combined to select the most satisfactory combination of the machining parameters from the initial optimal solutions.

As the spindle speed Ω and the tool life T_f reflect the energy consumption, they are combined with the optimization objectives absolute SLE and MRR to be the evaluation objectives. The dominance of one evaluation objective over another is determined by the advices of the experts. Then the judgement matrix $\boldsymbol{M}_A^*$ described in Eq. (32) is obtained. Therefore, based on the Eqs. (21) and (32), the calculated maximum real eigenvalue λ is 0.68 and the corresponding weight vector $\boldsymbol{W}$ for the four evaluation objectives is $\boldsymbol{W}$=[0.3936 0.3936 0.1375 0.0753].

$$\boldsymbol{M}_A^* = \begin{bmatrix} & \text{SLE} & \text{MRR} & \Omega & T_f \\ \text{SLE} & 1 & 1 & 3 & 5 \\ \text{MRR} & 1 & 1 & 3 & 5 \\ \Omega & 1/3 & 1/3 & 1 & 2 \\ T_f & 1/5 & 1/5 & 1/2 & 1 \end{bmatrix} \tag{32}$$

The specific values of the four evaluation objectives obtained from the information of the initial optimal solutions are listed in Table 3, and these values compose the decision-making matrix $D*$ shown in Eq. (33), as shown at the bottom of the next page. A data normalization described in Eqs. (24) and (25) is performed on the elements in matrix $D*$ to obtain the standard matrix $\boldsymbol{R}^*$ shown in Eq. (34), as shown at the bottom of the next page. Then the positive and negative bull's-eye solutions $\boldsymbol{R}^{*+}$ and $\boldsymbol{R}^{*-}$ can be obtained:

$$\begin{bmatrix} \boldsymbol{R}^{*+} \\ \boldsymbol{R}^{*-} \end{bmatrix} = \begin{bmatrix} 0.8469 & 0.9917 & 1 & 0.6260 \\ -1 & -1 & -0.7360 & -1 \end{bmatrix} \tag{35}$$

Therefore, with the weight vector $\boldsymbol{W}$, the deviations d_j^{*+} and d_j^{*-} of each solution are calculated and further used to obtain the fuzzy comprehensive membership degree of each solution shown in Eq. (36), as shown at the bottom of the next page. Comparing the values in the vector $\boldsymbol{u}$ to sort the initial optimal solutions, the results are listed in Table 3 and the fifth solution has the biggest value 0.676. Thus, the fifth one of the initial optimal solutions is determined as the most satisfactory solution.

C. COMPARISON STUDY

To further analyze the effects of the machining parameters on the surface location error SLE and material removal rate MRR, another two optimization models for the same milling process were established and solved to perform a comparison study. The multi-objective optimization model in section V-B is named as Model 1, and the other two mono-objective optimization models of minimum absolute SLE and maximum MRR respectively are named as Model 2 and Model 3. The two mono-objective optimization models are solved by a particle swarm optimization algorithm which has been presented in our prior work [36]. Results of the three optimization models are listed in Table 4.

TABLE 4. Comparisons of the three optimization results.

Objective	Spindle speed (rpm)	Cutting depth (mm)		Feed rate per tooth (mm/per)	Surface location error (μm)	Materials removal rate (10^5mm^3/min)	Tool life (min)
		Axial	Radial				
SLE and MRR	3379	6.56	5.69	0.20	32.56	1.01	85.70
SLE	5480	1.38	0.20	0.02	0.00002	0.0012	1374
MRR	3426	7.38	7.46	0.20	89.63	1.51	71.00

TABLE 5. The information of the machining parameters used in the milling experiments.

Order	Spindle speed (rpm)	Cutting depth (mm)		Feed rate per tooth (mm/per)	Surface location error (μm)		Error(%)
		Axial	Radial		Predicted	Experimental	
1	3379	6.56	5.69	0.20	32.56	34.69	6.14
2	3426	7.38	7.46	0.20	89.63	93.74	4.38
3	4500	8.80	2.90	0.17	56.40	52.87	-6.68
4	5200	4.20	16.40	0.12	75.14.	71.28	-5.42
5	6600	6.90	12.70	0.18	17.61	21.83	-5.24
6	7600	10.70	14.80	0.14	24.96	27.37	8.80
7	8300	9.10	3.20	0.08	41.09	38.32	-7.22
8	9600	10.80	9.80	0.10	107.96	115.35	6.41

When the optimization objective is minimum absolute SLE (Model 2), the obtained machining parameters (a_p, a_e and f_t) are much smaller than those obtained from the multi-objective optimization (Model 1) which minimizes the absolute SLE and maximizes the MRR simultaneously. However, the spindle speed is bigger than that of the Model 1, for the SLE is not linear to machining parameters. And their relationships are investigated in the following section V-D. In general, the smaller machining parameters can guarantee the part quality and tool life, but the MRR has a sharp decrease and results a lower machining efficiency.

When the optimization objective is maximum MRR (Model 3), the obtained machining parameters (n, a_p, a_e, f_t) are bigger than those of the multi-objective optimization (Model 1). However, with the increment of machining parameters and the MRR, the absolute SLE has a sharp increase and the tool life decreases for the tool wear is aggravated. The tool wear will increase the time and number of the tool-changing, resulting in more time-consumption for the whole machining process.

Comparing the results of the three models, the MRR and absolute SLE of Model 1 are between those of the Model 2 and Model 3. Therefore, the proposed multi-objective optimization model in this paper is effective in maximizing MRR and minimizing absolute SLE.

D. PARAMETRIC INFLUENCE ON ABSOLUTE SURFACE LOCATION ERROR

Since the MRR is linear to each machining parameter, influences of the spindle speed Ω, axial cutting depth a_p, radial cutting width a_e and feed rate per tooth f_t on the absolute SLE are only investigated in this section. Thus, variations of each machining parameter are determined to calculate the corresponding absolute SLEs. With the ranges of the machining parameters in Table 2, three specific values of the a_e are defined as 6, 12 and 18mm, and three specific

$$\boldsymbol{D}^* = \begin{bmatrix} (2.88\ 3.01\ 3.11\ 3.20\ 3.25\ 3.40\ 3.44\ 3.49\ 3.55\ 3.64\ 3.75\ 3.87\ 4.13\ 4.34\ 4.60\ 4.80\ 4.83\ 4.92\ 5.02\ 5.15) * 10^1 \\ (0.96\ 0.98\ 0.99\ 1.00\ 1.01\ 1.03\ 1.03\ 1.04\ 1.04\ 1.06\ 1.08\ 1.09\ 1.12\ 1.12\ 1.15\ 1.17\ 1.17\ 1.18\ 1.19\ 1.20) * 10^5 \\ (8.67\ 8.61\ 8.58\ 8.59\ 8.57\ 8.47\ 8.45\ 8.35\ 8.42\ 8.28\ 8.23\ 8.11\ 8.05\ 8.22\ 8.13\ 8.11\ 8.10\ 8.08\ 8.04\ 8.04) * 10^1 \\ (3.38\ 3.38\ 3.38\ 3.37\ 3.37\ 3.38\ 3.38\ 3.39\ 3.38\ 3.39\ 3.39\ 3.40\ 3.40\ 3.38\ 3.38\ 3.38\ 3.38\ 3.38\ 3.38\ 3.38) * 10^3 \end{bmatrix}^{\mathrm{T}} \tag{33}$$

$$\mathbf{R}^* = \begin{bmatrix} 0.85 & 0.74 & 0.66 & 0.58 & 0.54 & 0.42 & 0.39 & 0.35 & 0.30 & 0.22 & 0.13 & 0.04 & -0.17 & -0.35 & -0.55 & -0.72 & -0.74 & -0.82 & -0.89 & -1 \\ -1 & -0.83 & -0.75 & -0.67 & -0.59 & -0.42 & -0.42 & -0.34 & -0.34 & -0.17 & -0.004 & 0.08 & 0.33 & 0.33 & 0.58 & 0.74 & 0.74 & 0.83 & 0.91 & 0.99 \\ 1 & 0.85 & 0.76 & 0.78 & 0.72 & 0.45 & 0.41 & 0.12 & 0.32 & -0.07 & -0.19 & -0.54 & -0.71 & -0.23 & -0.49 & -0.53 & -0.55 & -0.61 & -0.74 & -0.73 \\ 0.14 & 0.14 & 0.25 & 0.63 & 0.57 & 0.25 & 0.25 & -0.24 & 0.36 & -0.24 & -0.40 & -1 & -1 & 0.03 & 0.03 & 0.08 & 0.03 & 0.08 & 0.03 & 0.03 \end{bmatrix}^{T} \tag{34}$$

$$\boldsymbol{u} = \begin{bmatrix} 5.79\ 6.02\ 6.10\ 6.56\ 6.76\ 6.52\ 6.25\ 5.42\ 6.22\ 5.36\ 5.53\ 3.93\ 4.00\ 5.04\ 4.89\ 4.95\ 4.75\ 4.76\ 4.63\ 4.59 \end{bmatrix}^{\mathrm{T}} * 10^{-1} \tag{36}$$

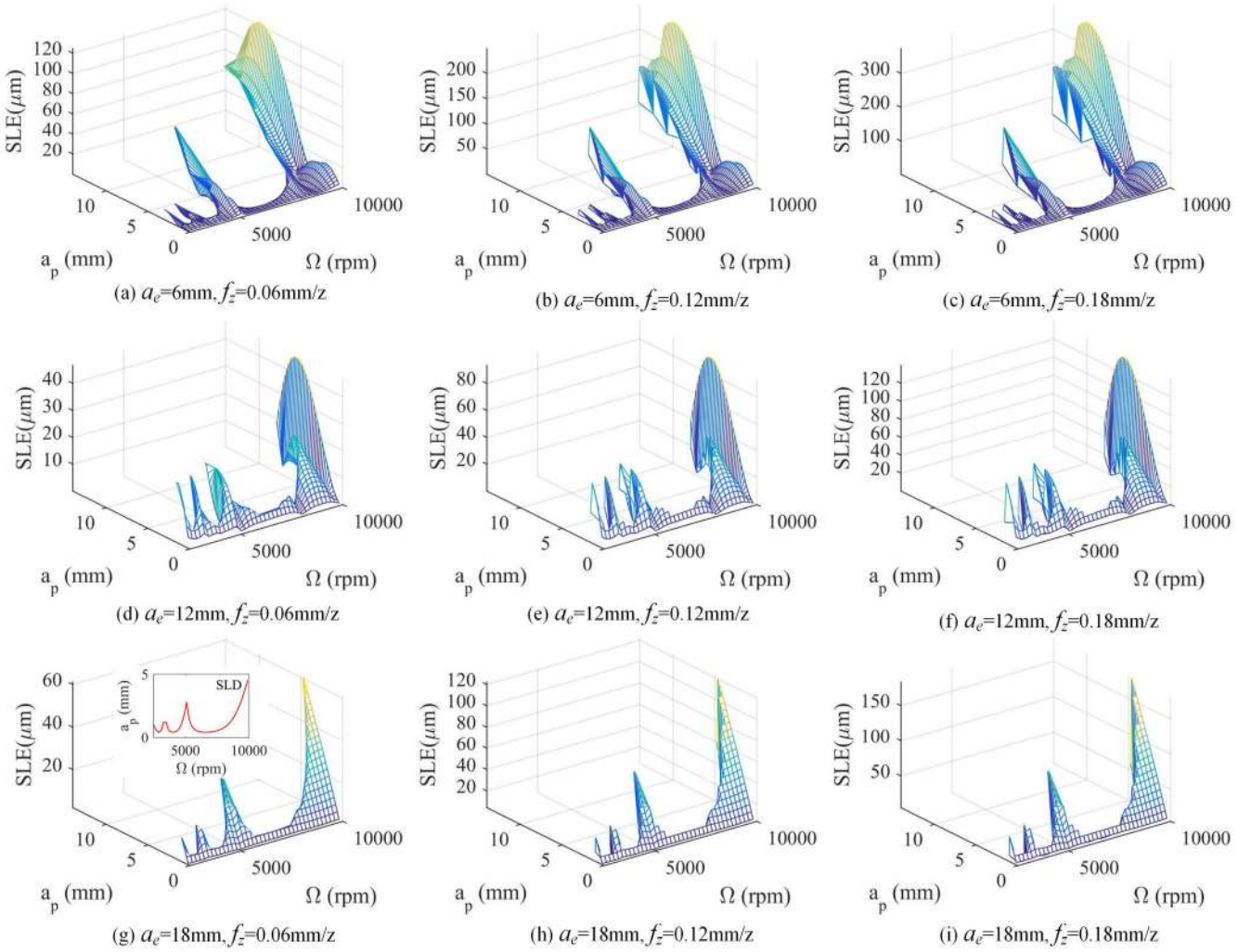

FIGURE 7. Influences of machining parameters on the SLEs.

values of the f_t are defined as 0.06, 0.12 and 0.18 mm/z. Then, 9 specific combinations of the a_e and f_t are determined. At each combination of a_e and f_t, the Ω and a_p vary within their ranges, and the a_p should be smaller than the limiting axial cutting depth a_{plim} to guarantee the machining stability. If a_p is bigger than a_{plim}, a_p will be substituted by a_{plim}.

Figure 7(a) to (i) are the three dimension (3D) surface graphs describing the changes of absolute SLE with the spindle speed and axial cutting depth at the defined specific combination of radial cutting width and feed rate per tooth. The graph has a shape similar with the stability lobe diagram (SLD) which describes the relationship between the Ω and a_{plim} (an example of the corresponding SLD shown in Fig. 7(g)), for the a_p is constrained to be smaller than or equal to the a_{plim} at each Ω. For any graph, it can be found that the absolute SLE trends to increase with the axial cutting depth at the specific value of Ω; however, with the increment of the spindle speed Ω, the absolute SLE is not always in a monotone increasing situation. Figure 7(a) to (c) are plotted when the a_e is 6mm, and the f_t are 0.06mm/z, 0.12mm/z, and 0.18mm/z respectively. Figure 7(d) to (f) are plotted when the a_e is 12 mm, and the f_t are 0.06mm/z, 0.12mm/z, and 0.18mm/z respectively. Figure 7(g) to (i) are plotted when the a_e is 18 mm, and the f_t are 0.06mm/z, 0.12mm/z, and 0.18mm/z respectively. It can be seen from these figures, when the a_e is a constant, the absolute SLE has a tendency to increase as the f_t increases; however, when the f_t is a constant, the absolute SLE does not increase as the a_e increases. Therefore, considering that these machining parameters not only affect the absolute SLE but also other optimization criterions (such as the MRR), the multi-objective optimization model is provided in this paper to give an efficient approach of obtaining an optimal machining parameters combination, which can realize a balance between the absolute SLE and other optimization objectives.

E. THE MILLING EXPERIMENT BASED ON THE MOST SATISFACTORY SOLUTION

To validate the predictions of the absolute SLE and verify the feasibility of the proposed multi-objective optimization

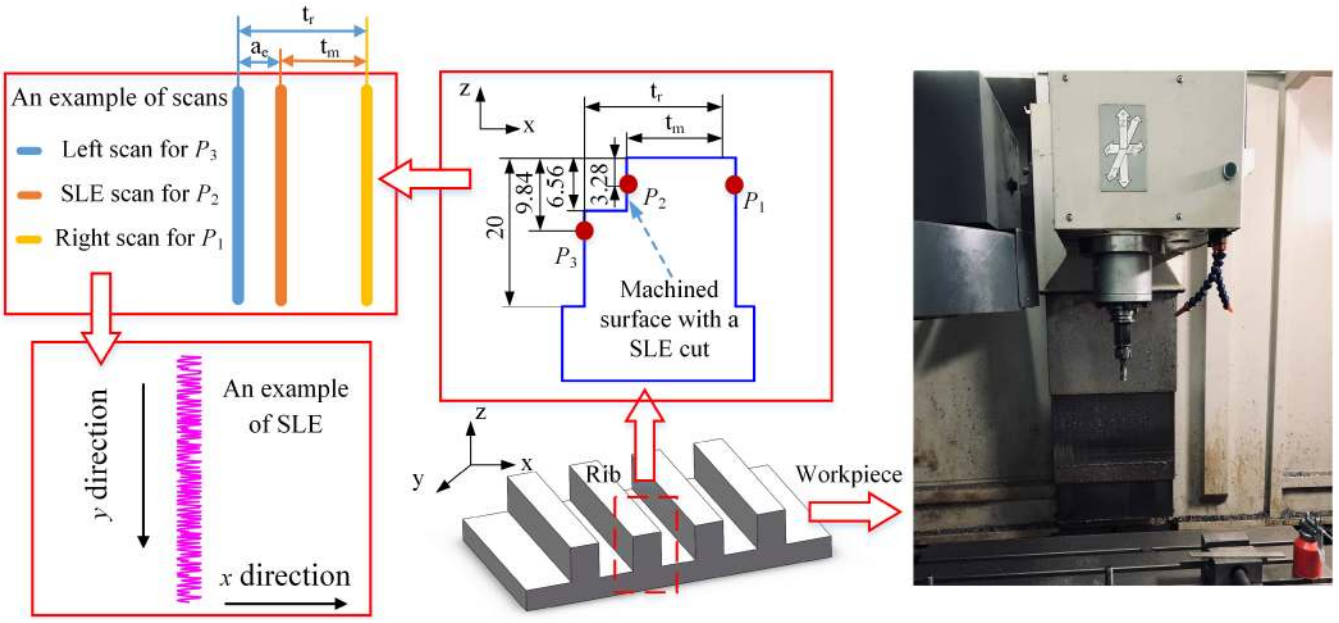

FIGURE 8. Information of the milling tests for validating the methods to predicted SLE.

model, eight combinations of machining parameters listed in Table 5 are determined to perform the milling experiments. The first two schemes in Table 5 are arranged according to the machining parameters calculated from the three optimization models shown in Table 4. Since the minimum absolute SLE 0.00002 μm of Model 2 is far smaller than the resolution and accuracy of the coordinate measuring machine (Zeiss, 2.1+ L/250$*\mu$m) used in the experiments, only the machining parameters of the Model 1 and Model 3 are selected. And the machining parameters of other six schemes are determined from the Fig. 7 randomly. During the milling process, the other milling conditions are kept the same as those described in section V-A.

The procedures to perform the milling tests and measure the SLEs are referring to the method proposed by Kiran *et al.* [19]. The workpiece mounted on the fixtures has four ribs whose basic dimensions are displayed in Fig. 8, and each rib is used to perform one milling test. Therefore, two workpieces are required to complete the eight milling tests. Before performing the cuts for the SLE tests, a finish pass was conducted on each side of the ribs at the axial depth of 20 mm to ensure that the surface is aligned with the coordinate frame of the vertical machining center. Then the defined eight milling tests were performed on the left sides of the ribs in order, and an example of the final dimensions of one rib is shown in Fig. 8.

The machined workpieces were used to measure the SLE of each rib with the aid of the coordinate measuring machine. The procedures for measuring the SLE of the first scheme in Table 5 are summarized and taken as an example as follows.

On each rib, three scans were selected. In Fig.8, the point P_1 is the projection of the scan whose displacement in z direction is 3.28 mm, and this scan is a reference scan located in the right side without a SLE cut; the points P_2 is the projection of the scan which locates on the machined surface after a SLE cut and is opposite to the previous scan; and the points P_3 is the projection of the scan whose displacement in z direction is 9.84 mm, and this scan locates on the left side of the rib and below the axial cutting depth 6.56mm of the SLE cut. The thicknesses obtained from these scans are used to calculate the SLE. One is the reference thickness t_r, which is the difference between the left scan at 9.84 mm and right scan at 3.28mm; and the other one is the measured thickness t_m based on the surface with a SLE cut, which is the difference between the left scan 3.28 mm and right scan 3.28 mm. Thus, the location error of one point SLE_p located at the scan with a SLE cut is obtained by the following equation:

$$\mathrm{SLE}_p = (t_r - t_m) - a_e \tag{37}$$

where a_e is the radial cutting width of the SLE cut, and only the information belonging to the steady-state (i.e., central) region of the three sans are used to calculate the SLE_p. Finally, the SLE is defined as the average value:

$$\mathrm{SLE}=\sum_{p=1}^{Num} \mathrm{SLE}_p \Big/ Num \tag{38}$$

where *Num* is the number of selected points.

According to Eq. (38), the measured SLEs for the 8 milling tests are listed in Table 5. Seen from Table 5, the absolute errors between the predicted and measured SLEs are

lower than nine percent and in an acceptable range. These errors may be ascribed to ignoring the workpiece flexibility in the SLE prediction algorithm, the measurement accuracy of the coordinate measuring machine, and the service state of the vertical machining center during real milling process. The first scheme listed in Table 5 is calculated from the multi-objective optimization model using the NSGA-II, AHP and GTD methods, and the corresponding small error 6.14% further validates the feasibility of the proposed multi-objective optimization model for selecting the optimal machining parameters at the process planning stage.

VI. CONCLUSION

Considering the influences of surface location error on the machining quality, this paper describes a method of predicting the surface location error in time domain, and then establishes a multi-objective optimization model to maximize the material removal rate and minimize the absolute surface location error simultaneously. In the multi-objective optimization model, the variables are the machining parameters including the spindle speed, axial cutting depth, radial cutting width and feed rate per tooth. The NSGA-II method is adopted to solve this multi-objective optimization model and obtain the Pareto-optimal solutions. Then the analytic hierarchy process and grey target decision methods are combined to find one most satisfactory solution from the Pareto-optimal solutions to balance the material removal rate and absolute surface location error.

A case study was performed on a vertical machining center to validate the feasibility of the proposed multi-objective optimization method. First, the impacting testing was performed on the tool tip to obtain the FRFs in x and y directions and identify the related modal parameters. Then, the multi-objective optimization model was established and solved by the NSGA-II method. Twenty solutions were selected from the obtained Pareto-optimal frontier and the fuzzy comprehensive membership degree of each solution was calculated. The fifth solution with the biggest degree 0.676 was determined as the most satisfactory optimal solution. The obtained MRR and absolute SLE of the multi-objective model were compared to the MRR and the SLE obtained from other two mono-objective models respectively, and the results show that the proposed multi-objective optimization method can realize a balance between two conflict objectives. Moreover, machining parameters of the most satisfactory optimal solution and seven other machining conditions were used to perform the milling tests. The SLEs were measured and compared to the predicted ones. The calculated errors were relatively small and in an acceptable range, validating the feasibility of the SLE prediction method and the multi-objective optimization method.

Therefore, considering that machining parameters have different influences on different optimization objectives, the proposed multi-objective optimization method can provide an effective approach to obtain a satisfactory machining parameters combination to balance the conflict objectives representing the machining efficiency and quality. In our future work, other factors affecting or reflecting the machining efficiency and quality, such as the workpiece system flexibility, tool wear, energy consumption and stochastic dynamic parameters, will be focused on to make the machining parameters optimization model more complete and more consistent with a real machining process.

REFERENCES

[1] G. Campatelli, L. Lorenzini, and A. Scippa, "Optimization of process parameters using a response surface method for minimizing power consumption in the milling of carbon steel," *J. Cleaner Prod.*, vol. 66, no. 1, pp. 309–316. Jun. 2014.
[2] X. Zhang and H. Ding, "Note on a novel method for machining parameters optimization in a chatter-free milling process," *Int. J. Mach. Tools Manuf.*, vol. 72, pp. 11–15, Sep. 2013.
[3] X. Chen, C. Li, J. Yan, and L. Li, "Optimization of cutting parameters with a sustainable consideration of electrical energy and embodied energy of materials," *Int. J. Adv. Manuf. Technol.*, vol. 96, pp. 775–788, Feb. 2018.
[4] O. Öz ahin, E. Budak, and H. N. Özgüven, "In-process tool point FRF identification under operational conditions using inverse stability solution," *Int. J. Mach. Tools Manuf.*, vol. 89, pp. 64–73, Feb. 2015.
[5] S. Paul and R. Morales-Menendez, "Active control of chatter in milling process using intelligent PD/PID control," *IEEE Access*, vol. 6, pp. 72698–72713, 2018.
[6] Y. T. Ic, E. S. Güler, C. Cabbaro lu, E. D. Yüksel, and H. M. Sa lam, "Optimisation of cutting parameters for minimizing carbon emission and maximising cutting quality in turning process," *Int. J. Prod. Res.*, vol. 56, no. 11, pp. 4035–4055, Jun. 2018.
[7] M. Solimanpur and F. Ranjdoostfard, "Optimisation of cutting parameters using a multi-objective genetic algorithm," *Int. J. Prod. Res.*, vol. 47, no. 21, pp. 6019–6036, Jan. 2009.
[8] A. Nair, P. Govindan, and H. Ganesan, "A comparison between different optimization techniques for CNC end milling process," *Procedia Eng.*, vol. 97, pp. 36–46, Jun. 2014.
[9] E. Budak and A. Tekeli, "Maximizing chatter free material removal rate in milling through optimal selection of axial and radial depth of cut pairs," *CIRP Ann.*, vol. 54, no. 1, pp. 353–356, Jan. 2005.
[10] J. Yan and L. Lin, "Multi-objective optimization of milling parameters—The trade-offs between energy, production rate and cutting quality," *J. Cleaner Prod.*, vol. 52, no. 4, pp. 462–471, Aug. 2013.
[11] Y. Zhang, Z. Pan, B. Li, and S. Liang, "Study on optimized principles of process parameters for environmentally friendly machining austenitic stainless steel with high efficiency and little energy consumption," *Int. J. Adv. Manuf. Technol.*, vol. 79, pp. 89–99, Jul. 2015.
[12] A. Zerti, M. A. Yallese, I. Meddour, S. Belhadi, A. Haddad, and T. Mabrouki, "Modeling and multi-objective optimization for minimizing surface roughness, cutting force, and power, and maximizing productivity for tempered stainless steel AISI 420 in turning operations," *Int. J. Adv. Manuf. Technol.*, vol. 102, pp. 135–157, May 2019.
[13] N. K. Sahu and A. B. Andhare, "Modelling and multiobjective optimization for productivity improvement in high speed milling of Ti–6Al–4V using RSM and GA," *J. Brazilian Soc. Mech. Sci. Eng.*, vol. 39, no. 12, pp. 5069–5085, Dec. 2017.
[14] M. Mia, P. R. Dey, M. S. Hossain, M. T. Arafat, M. Asaduzzaman, M. S. Ullah, and S. M. T. Zobaer, "Taguchi S/N based optimization of machining parameters for surface roughness, tool wear and material removal rate in hard turning under MQL cutting condition," *Measurement*, vol. 122, pp. 380–391, Jul. 2018.
[15] C. Li, X. Chen, Y. Tang, and L. Li, "Selection of optimum parameters in multi-pass face milling for maximum energy efficiency and minimum production cost," *J. Cleaner Prod.*, vol. 140, pp. 1805–1818, Jan. 2017.
[16] Y. Li and Q. Liu, "Service-oriented research on multi-pass milling parameters optimization for green and high efficiency," *J. Mech. Eng.*, vol. 11, pp. 89–98, Apr. 2015.
[17] S. P. L. Kumar, "Measurement and uncertainty analysis of surface roughness and material removal rate in micro turning operation and process parameters optimization," *Measurement*, vol. 140, pp. 538–547, Jul. 2019.

[18] T. Insperger, J. Gradisek, M. Kalveram, G. Stepan, K. Weinert, and E. Govekar, "Machine tool chatter and surface quality in milling processes," *Amer. Soc. Mech. Eng., Manuf. Eng. Division, MED*, vol. 15, no. 13, pp. 971–983, Nov. 2004.

[19] K. Kiran, M. Rubeo, M. C. Kayacan, and T. Schmitz, "Two degree of freedom frequency domain surface location error prediction," *Precis. Eng.*, vol. 48, pp. 234–242, Apr. 2017.

[20] B. P. Mann, B. T. Edes, S. J. Easley, K. A. Young, and K. Ma, "Chatter vibration and surface location error prediction for helical end mills," *Int. J. Mach. Tools Manuf.*, vol. 48, nos. 3–4, pp. 350–361, Mar. 2008.

[21] T. L. Schmitz and K. S. Smith, *Machining Dynamics: Frequency Response to Improved Productivity*. New York, NY, USA: Springer, 2009.

[22] T. L. Schmitz and B. P. Mann, "Closed-form solutions for surface location error in milling," *Int. J. Mach. Tools Manuf.*, vol. 46, nos. 12–13, pp. 1369–1377, Oct. 2006.

[23] X. Zhang, C. Xiong, Y. Ding, X. Huang, and H. Ding, "A synthetical stability method for cutting parameter optimization to assure surface location accuracy in flexible part milling," *Int. J. Adv. Manuf. Technol.*, vol. 75, pp. 1131–1147, Nov. 2014.

[24] X. Zhang, L. Zhu, D. Zhang, H. Ding, and Y. L. Xiong, "Numerical robust optimization of spindle speed for milling process with uncertainties," *Int. J. Mach. Tools Manuf.*, vol. 61, pp. 9–19, Oct. 2012.

[25] Z. Jiang, F. Zhou, H. Zhang, Y. Wang, and J. W. Sutherland, "Optimization of machining parameters considering minimum cutting fluid consumption," *J. Cleaner Prod.*, vol. 108, pp. 183–191, Dec. 2015.

[26] Y. Altintas, G. Stepan, D. Merdol, and Z. Dombovari, "Chatter stability of milling in frequency and discrete time domain," *CIRP J. Manuf. Sci. Technol.*, vol. 1, no. 1, pp. 35–44, Jun. 2009.

[27] I. P. Stanimirovic, M. L. Zlatanovic, and M. D. Petkovic, "On the linear weighted sum method for multi-objective optimization," *Facta Univ. Ser. Math. Inform.*, vol. 26, no. 4, pp. 49–63, 2011.

[28] H. Shimodaira, "Optimal design of generalized lapped orthogonal transforms: Multiobjective optimization techniques and experimental results," in *Proc. 5th Int. Symp. Multimedia Softw. Eng.*, Dec. 2003, pp. 102–109.

[29] P. K. Tripathi, S. Bandyopadhyay, and S. K. Pal. "Adaptive mufti-objective particle swarm optimization algorithm," in *Proc. IEEE Congr. Evol. Comput.*, Sep. 2007, pp. 2281–2288.

[30] Q. Yi, C. Li, Y. Tang, and X. Chen, "Multi-objective parameter optimization of CNC machining for low carbon manufacturing," *J. Cleaner Prod.*, vol. 95, pp. 256–264, May 2015.

[31] R. Dhabaler, S. J. VijayKumar, and T. P. Singh, "Multi-objective optimization of turning process during machining of AlMg1SiCu using non-dominated sorted genetic algorithm," *Procedia Mater. Sci.*, vol. 6, pp. 961–966, Jul. 2014.

[32] S. Chaki, R. N. Bathe, S. Ghosal, and G. Padmanabham, "Multi-objective optimisation of pulsed Nd:YAG laser cutting process using integrated ANN–NSGAII model," *J. Intell. Manuf.*, vol. 29, no. 1, pp. 175–190, Jan. 2015.

[33] S. Kannan, S. Baskar, J. D. McCalley, and P. Murugan, "Application of NSGA-II algorithm to generation expansion planning," *IEEE Trans. Power Syst.*, vol. 24, no. 1, pp. 454–461, Feb. 2009.

[34] L. F. de Oliveira Moura Santos, L. Osiro, and R. H. P. Lima, "A model based on 2-tuple fuzzy linguistic representation and analytic hierarchy process for supplier segmentation using qualitative and quantitative criteria," *Expert Syst. Appl.*, vol. 79, pp. 53–64, Aug. 2017.

[35] R. Li, Z. Jiang, C. Ji, A. Li, and S. Yu, "An improved risk-benefit collaborative grey target decision model and its application in the decision making of load adjustment schemes," *Energy*, vol. 156, pp. 387–400, Aug. 2018.

[36] C. Deng, J. Miao, G. Yin, L. Wang, Y. Feng, and Y. Zhao, "Study on prediction of machining stability for machine tool under operational state," *Adv. Eng. Sci.*, vol. 51, no. 3, pp. 184–191, May 2019.

CONGYING DENG received the Ph.D. degree in mechanical manufacturing and automation from Sichuan University, Chengdu, China, in 2016. She is currently an Associate Professor with the School of Advanced Manufacture and Engineering, Chongqing University of Posts and Telecommunications, Chongqing, China. She also does her postdoctoral research with Chongqing University, Chongqing. Her research interests include machine tool dynamics, high efficient machining, and CAD/CAE/CAM.

YI FENG received the B.E. degree in mechanical design manufacture and automation from the Chongqing University of Posts and Telecommunications, Chongqing, China, in 2017, where she is currently pursuing the M.S. degree with the School of Advanced Manufacturing Engineering.

JIANGUO MIAO received the M.S. degree in mechanical manufacturing and automation from Sichuan University, Chengdu, China, in 2017, where he is currently pursuing the Ph.D. degree in mechanical engineering with the School of Aeronautics and Astronautics. His current research interests include CNC machine tool cutting, signal processing and analysis, and fault diagnosis, prognosis, and health management.

YING MA received the B.E. degree in process equipment and control engineering from Sichuan University, Chengdu, China, in 2008, and the Ph.D. degree in mechanical engineering from Kansas State University, in 2016. She went to U.S. to pursue master and doctoral degrees, in 2009. She was a Lecturer with the School of Advanced Manufacture Engineering, Chongqing University of Posts and Telecommunications, Chongqing, China, in 2017.

BO WEI received the B.E. and Ph.D. degrees from the Beijing Institute of Technology, Beijing, China, in 2010 and 2016, respectively. Since 2016, she has been a Lecturer with the Chongqing University of Posts and Telecommunications, Chongqing, China. Her current research interests include space robot, biomimetic robot, and biological vision.